



Cite this: *Analyst*, 2019, **144**, 6609

A carbon dot-based fluorescent nanoprobe for the associated detection of iron ions and the determination of the fluctuation of ascorbic acid induced by hypoxia in cells and *in vivo*†

Yan Huang,^{‡a,b} Na He,^{‡b,c} Qi Kang,^{*a} Dazhong Shen,^{id a} Xiaoyan Wang,^{b,c} Yunqing Wang^b and Lingxin Chen^{id *b,c,d}

Maintaining the redox balance of biological systems is a key point to maintain a healthy physiological environment. Excessive iron ions (Fe^{3+}) can cause apoptosis, tissue damage and death. Fortunately, ascorbic acid (AA) as a reducing agent has been evaluated for the reduction of Fe^{3+} . Moreover, AA plays an important role in relieving hypoxia-induced oxidative stress. Therefore, the real-time imaging of the Fe^{3+} and AA fluctuations is important for understanding their biofunctions in cells and *in vivo*. In this work, we developed a fluorescent nanoprobe carbon dot-desferrioxamine B (CD-DB) by the conjugate connection of CDs and desferrioxamine B (a complexing agent for Fe^{3+}) for the associated detection of Fe^{3+} and AA. CD-DB exhibited excellent sensitivity and selectivity for the detection of Fe^{3+} and AA. The nanoprobe CDs-DB@Fe obtained by the reaction of CD-DB and Fe^{3+} was suitable for tracing the dynamic changes of AA in cells and *in vivo*. Therefore, CDs-DB@Fe was used for monitoring the fluctuation of AA in hypoxic cell models, hypoxic zebrafish models and liver ischemia mice models. These results exhibited the decrease in AA under hypoxic conditions because AA was consumed to neutralize free radicals and relieve hypoxia-induced oxidative stress damage. The ideal biocompatibility and low toxicity make our nanoprobe a potential candidate for the research of the physiological effects of AA *in vivo*.

Received 31st August 2019,
Accepted 16th September 2019

DOI: 10.1039/c9an01694e

rs.c.li/analyst

1. Introduction

Iron ions (Fe^{3+}) are one of the most important trace elements *in vivo* and play significant roles in physiological processes, such as oxygen uptake, oxygen metabolism and electronic transfer.^{1–3} Many structural units in the form of an iron complex involve the process of transporting and exchanging oxygen, and several enzymes contain Fe^{3+} as a part of the catalytic sites.⁴ Excessive Fe^{3+} causes many diseases, including cancer, organ dysfunction, organ failure, tissue damage and

even death.^{5–8} Fortunately, ascorbic acid (AA), also known as vitamin C, can rapidly reduce Fe^{3+} to Fe^{2+} to mitigate the damage of Fe^{3+} . AA is often used in health care supplements as an antioxidant.^{9,10} As is well-known, AA is a highly active reducing agent, and it can effectively eliminate free radicals and relieve oxidative stress.^{11,12} Besides, it is a vital vitamin in the diet of humans and has been used for the prevention and treatment of common cold, mental illness, cancer and so on.^{13,14} So far, there are some methods to detect AA and research its biological functions; these include high-performance liquid chromatography (HPLC)/UV spectroscopy,¹⁵ ^{13}C nuclear magnetic resonance spectroscopy (^{13}C NMR)/HPLC¹⁶ and liquid chromatography/mass spectrometry (LC/MS).¹⁷ However, these technologies are not suitable for studying the biological activity of AA due to the destruction of the sample and the irreversible damage. In addition, the highly active AA can be easily destroyed and oxidized by air during the process of sample treatment. Therefore, these technologies cannot realize the real-time and accurate detection of AA in living cells and *in vivo*. The fluorescence detection technology using fluorescent nanoprobe exhibits various advantages for the detection of intracellular reactive species, which include greater sensitivity, excellent selectivity, more convenience, less invasive-

^aCollege of Chemistry, Chemical Engineering and Materials Science, Key Laboratory of Molecular and Nano Probes, Ministry of Education, Shandong Normal University, Jinan 250014, China. E-mail: kangqi@sdsnu.edu.cn

^bCAS Key Laboratory of Coastal Environmental Processes and Ecological Remediation, The Research Center for Coastal Environmental Engineering and Technology, Yantai Institute of Coastal Zone Research, Chinese Academy of Sciences, Yantai 264003, China. E-mail: lxchen@yic.ac.cn

^cSchool of Pharmacy, Binzhou Medical University, Yantai 264003, China

^dCollege of Chemistry and Chemical Engineering, Qufu Normal University, University, Qufu 273165, China

†Electronic supplementary information (ESI) available. See DOI: 10.1039/C9AN01694E

‡These authors contributed equally.

ness, and real-time imaging.^{18–20} Therefore, the development of an effective nanoprobe that has high sensitivity and selectivity for the detection and imaging of excessive Fe³⁺ and AA is necessary.

The development of fluorescent nanomaterials has been very quick and has been applied to the field of analysis and medicine, including quantum dots (QDs),^{21,22} carbon dots (CDs)^{23,24} and precious metal nanoclusters.²⁵ Among them, CDs have attracted researchers' extensive attention due to their stable photoluminescence, high quantum yield, low toxicity and suitable biocompatibility.^{26–28} Hence, CDs have an excellent potential for the diagnosis and treatment of diseases. Actually, CDs have been widely applied in bioimaging^{29–31} and the design of sensors for the detection of pH,^{32–34} ions (such as Hg²⁺, Cu²⁺, Ag⁺, Fe³⁺, and PO₄^{3–})^{35–41} and molecular substances (for instance, DNA, nitrite, glucose, and biethiol)^{42–44} by monitoring the change in the fluorescence intensity. Recently, some nanoprobe based on CDs,^{45–47} graphene quantum dots (GQDs),⁴⁸ gold nanoclusters (AuNCs)⁴⁹ and graphitic carbon nitride nanosheets (g-C₃N₄ NNs)⁵⁰ have been reported for the detection of Fe³⁺ and AA. These detection methods have high quantum yields, high sensitivity and excellent anti-salt ability.^{45–50} However, some questions also exist in the previous studies: (1) there is a lack of a ligand for fixing Fe³⁺, which produces non-ideal selectivity; (2) only few of them are applied in actual biological samples (in living cells and *in vivo*); (3) due to the lack of applications in clinical models, no related nanoprobe has been applied in clinical diagnosis. These problems have hindered the progress of the application of such nanoprobe. In addition, the comparison of such recently reported nanoprobe is shown in Table S1.†

The inner filter effect (IFE), an effective mechanism for fluorescence analysis, was used for the design of the fluorescent nanoprobe. This mechanism has high sensitivity because the changes in the absorption of the nanoprobe can exponentially transform to fluorescence intensity.^{51–53} In this study, we revised a previous synthetic method for the simple one-pot synthesis of CDs, and the CDs were quenched by Fe³⁺ due to IFE.^{50,54} Desferrioxamine B, a complexing agent for Fe³⁺, conjugated to the surface of CDs to obtain our nanoprobe carbon dot-desferrioxamine B (CD-DB). Then, Fe³⁺ could be reduced to Fe²⁺ by AA, leading to the restoration of fluorescence. Therefore, CD-DB could be used for associatively detecting Fe³⁺ and AA. As a potential nanoprobe, CD-DB exhibited outstanding sensitivity and selectivity for the detection of Fe³⁺ and AA *in vitro*. The bioassays demonstrated that CD-DB could associatively detect Fe³⁺ and AA in living cells. Furthermore, CDs-DB@Fe (CD-DB combined with Fe³⁺) was successfully applied to monitor the fluctuation of AA in hypoxic cell models, hypoxic zebrafish models and liver ischemia-induced hypoxic mice models. To the best of our knowledge, this is the first time that a CD-based nanoprobe is applied to analyze the changes in AA in a hypoxic biological sample. Western blot and TUNEL assays were also performed to demonstrate these results. Overall, we hope that our nanoprobe can be applied to clarify the redox dynamic

process of AA in biological systems and even in clinical diagnosis.

2. Experimental

2.1 Synthetic procedures of nanoprobe

2.1.1 Synthesis of CDs. Citric acid (5 g, 46.9 mmol) was added to a crucible, and the crucible was heated from room temperature to 300 °C by a muffle furnace for 2 h. Then, a fluffy black solid was obtained, and the crucible was cooled to room temperature. The product, which was a black solid, was combined with 25 mL water and a brown dispersion appeared. This mixture was placed in a dialysis bag (cutoff M_n : 1.0 kDa) and dialyzed against water for 2 days to remove small molecules. Finally, CDs were dried *in vacuo* to give a dark brown solid.

2.1.2. Synthesis of CDs-DB. The CDs (10 mg) was dissolved in 10 mL ultra-pure water with the solution under Ar gas flow to ensure the removal of oxygen. Then, EDC (11.5 mg, 0.06 mmol) and NHS (6.9 mg, 0.06 mmol) were added to the abovementioned solution and stirred for 30 min at room temperature. Desferrioxamine B (10 mg, 0.018 mmol) was added to the abovementioned solution and stirred for 24 h at room temperature under dark conditions. The final solution was then dialyzed by a dialysis bag (cutoff M_n : 1.0 kDa) against water for 3 days to remove the unreacted molecular precursors. Finally, the water in the dialyzate was lyophilized and CD-DB was obtained as a brown powder.

2.2 Cell staining procedures

HepG2 cells were seeded in a flat-bottom 6-well plate with glass coverslips in 2 mL culture medium. After overnight incubation, the cells were treated with CDs-DB@Fe for 1 h at 37 °C. Then, the treated cells were cultivated with AA (1 mM) for 1 hour. The cells were washed by PBS buffer for three times. Subsequently, the cells were imaged under a laser scanning confocal microscope. Cells were incubated with pure CDs-DB@Fe for 1 h as a control. The excitation wavelength of the HepG2 cells was 405 nm, and the emission was collected from 420 nm to 500 nm.

2.3 Hypoxic conditions in cell and zebrafish incubation

First, 1 mM AA was added to cells and zebrafish. Then, 0.1% O₂ concentration was generated with AnaeroPack™ (Mitsubishi Gas Chemical Company, Co. Inc., Japan). Also, 1–20% O₂ concentration was generated with a multi gas incubator (Sanyo) by means of N₂ substitution.

2.4 Establishment of the liver ischemia mice model and imaging of liver ischemia tissue sections

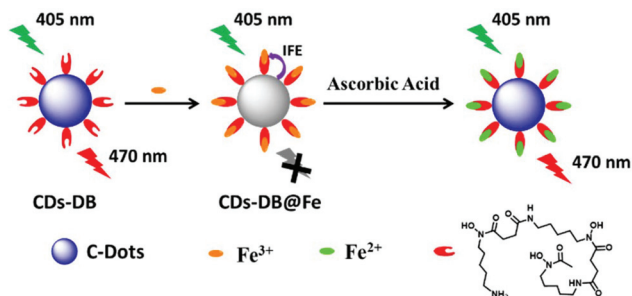
Six to eight week-old BALB/c mice were obtained from Binzhou Medical University. Mice were group-housed on a 12 : 12 light–dark cycle at 22 °C with free access to food and water (1 mM AA was dissolved in water). BALB/c mice, 20–25 g, were selected and divided into different groups. Mice without any treatment

were used as the control group. Mice were fasted for 12 h with free access to water before liver ischemic surgery. First, the mice were anesthetized by intraperitoneal injection of 3% pentobarbitalum natricum (80 mg kg^{-1}) dissolved in saline and then, the hairs on the abdomen of the mice were shaved and disinfected using 75% ethanol. The left and middle lobes of the liver were separated after dissecting the abdominal cavity to close the portal vein and hepatic artery using a non-invasive vascular clip. After 0.5 min, the whitened left and middle lobes of the liver were observed to confirm that liver ischemia was successful. Persistent ischemia was observed for 0.5 min, 5 min, 10 min, 30 min and 60 min; then, the ischemic liver tissues were dissected to frozen sections. The entire process of ischemia in mice was conducted on a 37°C heating plate. Next, the liver ischemia tissue sections were treated with 0.1 mg mL^{-1} CDs-DB@Fe for 1 h and then washed with PBS buffer ($\text{pH} = 7.4$) to remove excess CDs-DB@Fe. Then, the sections were imaged under a laser scanning confocal microscope. All experimental procedures were conducted in conformity with the institutional guidelines for the care and use of laboratory animals, and the protocols were approved by the Institutional Animal Care and Use Committee in Binzhou Medical University, Yantai, China (Approval Number: No. BZ2014-102R).

3. Results and discussion

3.1 Design strategies and characterization of nanoprobe CD-DB

The synthetic approaches of the multi-response fluorescent nanoprobe CD-DB are outlined in Scheme S1.† The multi-response mechanism for the nanoprobe is shown in Scheme 1. We used a simple one-step method to directly synthesize fluorescent carbon dots using citric acid as the raw material. This is a green chemistry synthesis method because no toxic chemicals were generated. The CDs have a reactive group ($-\text{COOH}$) to provide sites for modification; moreover, the fluorescent CDs have a high quantum yield. Furthermore, desferrioxamine B is a complexing agent that can specifically bind Fe^{3+} . We synthesized CD-DB through the reaction between the carboxyl group on CDs and the amino group on desferrioxamine B to form an amide bond. Because of the inner filter effect (IFE),⁴⁵



Scheme 1 The multi-response mechanism for the nanoprobe.

the fluorescence signal of CD-DB could be quenched by Fe^{3+} , and Fe^{3+} could be reduced to Fe^{2+} via highly reductive AA, which led to the restoration of the fluorescence signal. Therefore, our dual-response nanoprobe CD-DB could detect Fe^{3+} and AA. As is well-known, Fe^{3+} can be reduced by AA, which widely exists in living cells and *in vivo*. Hence, CDs-DB@Fe obtained from the reaction between CD-DB and Fe^{3+} could be a powerful tool for the detection of AA in living cells and *in vivo*. The construction of a dual-response nanoprobe has a great potential for the non-invasive detection of AA *in vivo* and can even be applied in disease detection.

The transmission electron microscopy (TEM) images and mean particle size distribution clearly indicated that the synthesized CD-DB was spherical in shape with an average size of 2.9 nm (Fig. 1a and b). The surface status information on CD-DB was analyzed from the FT-IR spectra (Fig. 1c). The following information was analyzed: the stretching vibrations of C–N at 1422 cm^{-1} and the vibrational absorption band of C=O at 1679 cm^{-1} . The broad absorption bands at $3100\text{--}3500 \text{ cm}^{-1}$ were attributed to the stretching vibrations of O–H and N–H. These absorption bands suggested that many amino functional groups and hydroxyl groups were distributed on the surface of CD-DB, leading to CD-DB having good water solubility.

3.2 Spectroscopic properties toward Fe^{3+} and AA

The previous experiment illustrated that the nanoprobe CD-DB and CDs-DB@Fe would work well under physiological conditions ($\text{pH} = 7.4$) (ESI†). The pH values hardly affected the fluorescence intensity of CD-DB and CDs-DB@Fe. The results indicated that our nanoprobe would be suitable for applications in living cells and *in vivo*. As shown in Fig. 2a and b, CD-DB (0.1 mg mL^{-1}) displays obvious absorption and fluorescence emission profiles at 350 nm ($\epsilon_{350 \text{ nm}} = 2.9 \times 10^4 \text{ M}^{-1} \text{ cm}^{-1}$) and 470 nm, respectively. On increasing the concentrations of Fe^{3+} ($0\text{--}45 \mu\text{M}$) in the CD-DB aqueous solution, the fluorescence signal of CD-DB was quenched due to IFE and formed CDs-DB@Fe. We then established a quantitative linear relationship between the fluorescence intensity ($F_{470 \text{ nm}}$) and Fe^{3+} concentrations. From Fig. 2c, we can infer that our nanoprobe is suitable for Fe^{3+} detection. The regression equation was $F_{470 \text{ nm}} = -2.22 \times 10^4 [\text{Fe}^{3+}] \mu\text{M} + 1.16 \times 10^6$, with $r = 0.9930$. The limit of detection was 45 nM ($3\sigma/k$, where σ is the standard deviation of the blank measurement, and k is the

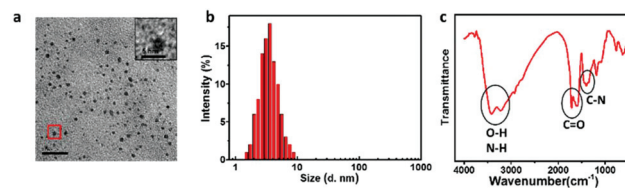


Fig. 1 Characterization of nanoprobe CD-DB. TEM imaging (a) and the mean particle size distribution (b) of CD-DB. (c) FT-IR spectrum of nanoprobe CD-DB.

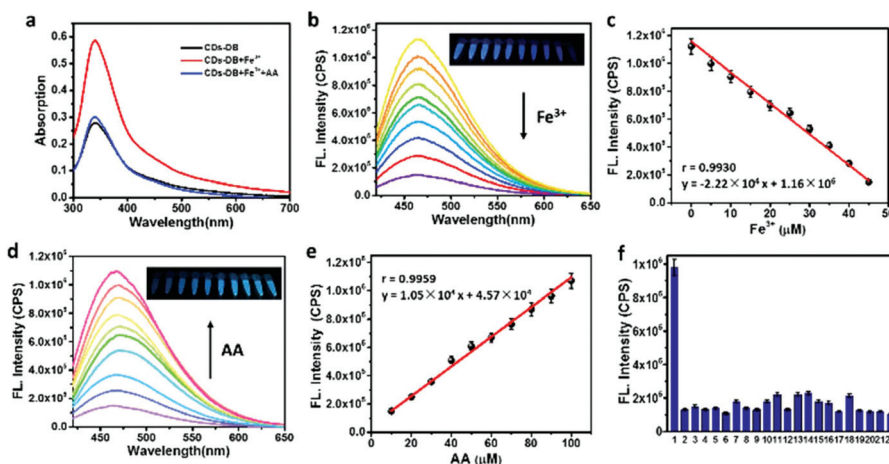


Fig. 2 Spectral properties of CD-DB and CDs-DB@Fe. (a) Absorption spectral changes of CD-DB ($10 \mu\text{g mL}^{-1}$) in the presence of Fe^{3+} ($45 \mu\text{M}$) or AA ($100 \mu\text{M}$) in HEPES (pH 7.4, 10 mM) at 37°C . (b) Fluorescence emission spectral changes of CD-DB ($10 \mu\text{g mL}^{-1}$); spectra were acquired after 10 min upon addition of various concentrations of Fe^{3+} (0– $45 \mu\text{M}$). (c) The plot of the linear relationship between fluorescence intensities and Fe^{3+} concentrations (0– $45 \mu\text{M}$). (d) Fluorescence emission spectral changes of CDs-DB@Fe ($10 \mu\text{g mL}^{-1}$); spectra were acquired after 10 min upon addition of various concentrations of AA (10– $100 \mu\text{M}$). (e) The plot of the linear relationship between fluorescence intensities and AA concentrations (10– $100 \mu\text{M}$). (f) Fluorescence response of CDs-DB@Fe ($10 \mu\text{g mL}^{-1}$) to AA and various biospecies ($100 \mu\text{M}$). 1. AA, 2. vitamin A, 3. vitamin B1, 4. vitamin B2, 5. vitamin B6, 6. biotin, 7. folic acid, 8. vitamin B12, 9. inositol, 10. vitamin D, 11. tocopherol, 12. vitamin K, 13. glutathione, 14. L-cysteine, 15. tryptophan, 16. glycine, 17. alanine, 18. cystine, 19. leucine, 20. L-serine, 21. histidine, 22. Blank. All data were acquired in 10 mM HEPES (pH 7.4) at 37°C after being maintained for 10 min ($\lambda_{\text{ex}} = 405 \text{ nm}$, $\lambda_{\text{em}} = 470 \text{ nm}$).

slope of the regression equation), and the experimental detection limit was $0.1 \mu\text{M}$.

It is noteworthy that the quenched fluorescence of CDs-DB@Fe could be recovered upon the addition of AA. Thus, CDs-DB@Fe was incubated with increasing concentrations of AA (10– $100 \mu\text{M}$). As shown in Fig. 2d, since Fe^{3+} is reduced to Fe^{2+} and the IFE process is removed, the fluorescence maximum at 470 nm strongly increases. To assess the ability of CDs-DB@Fe for the detection of AA, the fluorescence emission at 470 nm was observed to exhibit a linear relationship with AA concentrations (Fig. 2e), which revealed the ability of CDs-DB@Fe for the quantitative and qualitative detection of AA. The regression equation was $F_{470 \text{ nm}} = 1.05 \times 10^4 [\text{AA}] \mu\text{M} + 4.57 \times 10^4$, with $r = 0.9959$. The limit of detection was calculated to be 80 nM ($3\sigma/k$), and the experimental detection limit was measured to be $0.2 \mu\text{M}$ under the experimental conditions. The photographs of the effect of different concentrations of Fe^{3+} and AA on the fluorescence intensity of the nanoprobe are shown in Fig. 2b and d. These results demonstrated that our nanoprobe could monitor Fe^{3+} /AA concentrations, which made our nanoprobe a potential tool for applications in cells.

3.3 Selectivity to Fe^{3+} and AA

To verify the fluorescence response to other metal ions, we tested the selectivity of CD-DB against common metal ions and that of CDs-DB@Fe against amino acids and vitamins in HEPES solutions (10 mM, pH 7.4). Compared to other metal ions, CD-DB offered remarkable fluorescence quenching for Fe^{3+} . Fig. S3† demonstrates that Cd^{2+} , Zn^{2+} , Co^{2+} , Ni^{2+} , Pb^{2+} , Fe^{2+} , Cu^{2+} , Ca^{2+} , Ag^+ , Mg^{2+} , Mn^{2+} and Hg^{2+} cause almost no response in the emission signal after 20 min incubation. The

results showed that CD-DB had good selectivity for Fe^{3+} detection over other common metal ions. The fluorescence responses of CDs-DB@Fe to other amino acids and vitamins were also evaluated (Fig. 2f). CDs-DB@Fe (0.1 mg mL^{-1}) could provide an obvious fluorescence response to AA. However, no obvious changes in the spectra were observed upon the addition of vitamin A, vitamin B1, vitamin B2, vitamin B6, biotin, folic acid, vitamin B12, inositol, vitamin D, tocopherol, vitamin K, glutathione, L-cysteine, tryptophan, glycine, alanine, cystine, leucine, L-serine and histidine. As shown in Fig. S4,† no obvious changes in the fluorescence intensity can be observed upon the addition of OH^- , NO_3^- , SO_4^{2-} , HSO_4^- , CO_3^{2-} , HCO_3^- , SO_3^{2-} , HSO_3^- , ClO^- , PO_4^{3-} , F^- , Cl^- , Br^- and I^- . These results demonstrated that CDs-DB@Fe was a highly selective fluorescent nanoprobe for AA detection over other amino acids, anions and vitamins. Taken together, these kinetic and selectivity assays revealed that our nanoprobe could work well under physiological conditions for the investigation of Fe^{3+} and AA.

3.4 Imaging of cell response to Fe^{3+} and AA and organelle localization

Encouraged by the sensitive and selective detection of Fe^{3+} and AA with our nanoprobe, we tried to exploit the potential applications for Fe^{3+} and AA detection in cells and *in vivo*. Therefore, we first performed a standard MTT assay to evaluate the cytotoxicity of CD-DB and CDs-DB@Fe. As demonstrated in Fig. S5 and S6,† more than 90% of the HepG2 cells survived after the cells were incubated with CD-DB (0– $200 \mu\text{g mL}^{-1}$) for 24 h; moreover, more than 80% of the HepG2 cells survived after the cells were incubated with CDs-DB@Fe (0– $200 \mu\text{g}$

mL^{-1}). The 50% cell survival concentration value (IC_{50}) was predicted to be 2.0 mg mL^{-1} for CD-DB and 1.7 mg mL^{-1} for CDs-DB@Fe, which indicated the low cytotoxicity of CD-DB and CDs-DB@Fe.

We next investigated the ability of CD-DB for Fe^{3+} and AA detection in living cells. The HepG2 cell line was chosen as the test model. First, the cells were incubated with $10 \mu\text{g mL}^{-1}$ CD-DB for 1 h at 37°C as a control. The cells showed a strong fluorescence signal (Fig. 3a) and then, $50 \mu\text{M Fe}(\text{NO}_3)_3$ was added to the cells and treated for 10 min. As shown in Fig. 3a, the cells display apparently quenched fluorescence, which indicated that CD-DB could detect the additional Fe^{3+} ions in living cells. Next, the cells were incubated with $50 \mu\text{M AA}$ for

another 10 min, and the fluorescence intensity rose to a plateau rapidly (Fig. 3a). Then, the cells were treated with CD-DB under continuous laser irradiation for 1 h, and the cells still exhibited strong fluorescence intensity. These results indicated that CD-DB could be successfully applied to monitor Fe^{3+} and AA, and CD-DB also had good light stability in living cells.

To verify how CD-DB was internalized by the cells, a co-localization experiment was carried out by co-staining the HepG2 cells with CD-DB and LysoTracker Green DND-26 (a commercial Lyso-Tracker). The tested cells were incubated with $10 \mu\text{g mL}^{-1}$ CD-DB for 1 h at 37°C before imaging; then, the cells were treated with $1 \mu\text{g mL}^{-1}$ LysoTracker for 15 min. For the CD-DB fluorescent channel, a strong fluorescence signal appeared in the cells. Lysosomes were stained by LysoTracker and exhibited a clear fluorescence signal at the green channel (570–650 nm) under the excitation of 559 nm. The merged image of the CD-DB fluorescent channel and lysosomes mainly shows an orange fluorescence signal (Fig. 3b), which indicates that the fluorescence signals at the two channels overlap well in discrete subcellular locations. We acquired the Pearson's coefficient ($r = 0.95$), implying the preferential distribution of CD-DB in lysosomes. Simultaneously, the intensity profiles of the linear regions of interest (white line in Fig. 3b) across the HepG2 cells were in close synchrony. A large amount of CD-DB was observed to accumulate in the lysosomes in the cells, indicating that CD-DB might be ingested *via* endocytosis.

Since AA cannot be generated in living cells and *in vivo*, we added 1 mM AA to the cells before imaging and employed the nanoprobe CDs-DB@Fe to study its physiological function. Pan *et al.* reported the metabolic way of AA under normoxia and hypoxia conditions.⁵⁵ As is well-known, AA is a reducing agent (antioxidant) that can neutralize free radicals and relieve oxidative stress. Therefore, CDs-DB@Fe was employed as the nanoprobe to detect the fluctuation of AA under a hypoxia condition. Initially, the HepG2 cells were cultured under hypoxic conditions with 20%, 10%, 5%, 1%, and 0.1% O_2 for 4 h; then, the cells were incubated with $10 \mu\text{g mL}^{-1}$ CDs-DB@Fe for 1 h at 37°C . As shown in Fig. 3c, strong fluorescence images were acquired from the cells cultured with 20% and 10% O_2 , while the signal was quite weak under 1% and 0.1% O_2 conditions. These results revealed that the content of AA decreased in living cells under hypoxic conditions due to the consumption of free radicals. A laser scanning confocal microscope is valuable for relatively small amounts of cells only in visual fields, which might decrease the reliability of the data owing to various uncontrolled factors. A flow cytometry assay can provide more statistically reliable data by analyzing millions of cells rapidly and sensitively,⁵⁶ which has been highly needed. Furthermore, all the fluorescence data were verified *via* a flow cytometry assay (Fig. 3c). In addition, the expression of the hypoxia inducible factor 1- α (HIF-1 α) was examined using western blot analysis to exhibit the hypoxic cell model. The expression of HIF-1 α was evidently upregulated under hypoxia stress (Fig. 3d). These data demonstrated that CDs-DB@Fe was

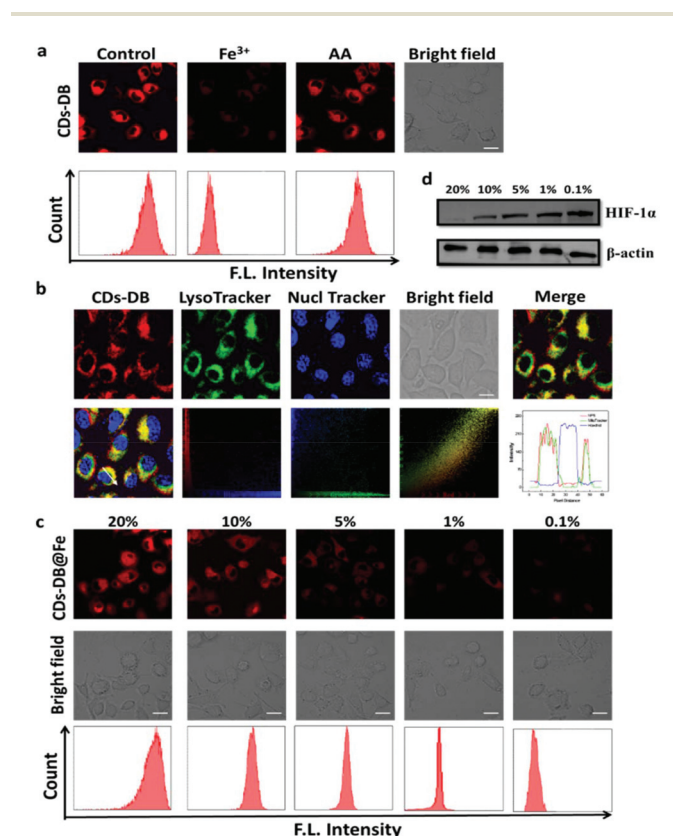


Fig. 3 Fluorescence imaging and flow cytometry assay in living HepG2 cells to detect Fe^{3+} and AA with CD-DB ($10 \mu\text{g mL}^{-1}$); then, the cells were washed with DMEM to remove the redundant CD-DB. Images display emission from 450 to 550 nm upon excitation at 405 nm. (a) HepG2 cells were incubated with CD-DB for 1 h and then, $50 \mu\text{M Fe}(\text{NO}_3)_3$ was added. After 10 min, $50 \mu\text{M AA}$ was added to the cells. (b) Lysosome localization of CD-DB was determined by co-stained CD-DB with lysosome trackers (Lyso Tracker) in HepG2 cells (red channel: $\lambda_{\text{ex}} = 405 \text{ nm}$, $\lambda_{\text{em}} = 450\text{--}550 \text{ nm}$). LysoTracker showing lysosomes (green channel: $\lambda_{\text{ex}} = 559 \text{ nm}$, $\lambda_{\text{em}} = 570\text{--}650 \text{ nm}$). Organelle Lights NE-GFP showing nuclei (blue channel: $\lambda_{\text{ex}} = 488 \text{ nm}$, $\lambda_{\text{em}} = 500\text{--}550 \text{ nm}$). (c) Fluorescence imaging of the HepG2 cells by CDs-DB@Fe under hypoxic conditions with 20%, 10%, 5%, 1%, and 0.1% O_2 for 4 h (emission collected from 450 to 550 nm upon excitation at 405 nm). (d) Western blotting analysis of HIF-1 α at different O_2 concentrations, where β -actin was used as a loading control. Images are representative of $n = 5$ independent experiments. Scale bar: $10 \mu\text{m}$.

valuable for the detection of intracellular AA, and AA decreased under hypoxic conditions.

3.5 Imaging of zebrafish under hypoxic conditions

Since CDs-DB@Fe was successfully applied to monitor AA in living cells, we next strived to investigate the detection of AA in larval (7 days post fertilization) zebrafish under hypoxic conditions. At this stage in their development, zebrafish were approximately 3 mm in length and maintained a high level of transparency. We first tested the toxicity of CDs-DB@Fe for zebrafish. By monitoring the zebrafish for 7 days (Fig. 4b), it was observed that no zebrafish died after they were incubated with 1 mg mL^{-1} CDs-DB@Fe, which indicated the negligible toxicity of CDs-DB@Fe. The zebrafish models were incubated with a multi-gas incubator (Sanyo) by means of N_2 substitution under 20%, 10%, 5% and 1% O_2 for 4 h. Then, the zebrafish were incubated with 0.1 mg mL^{-1} CDs-DB@Fe for 1 h. The imaging of zebrafish was obtained by a laser scanning confocal microscope. As expected, the zebrafish under 20% and 10% O_2 showed a strong fluorescence signal, and the fluorescence signal significantly decreased under 5% and 1% O_2 . All these results demonstrated that AA decreased in the zebrafish under hypoxic conditions due to the hypoxia-induced oxidative stress. In addition, our nanoprobe CDs-DB@Fe was found to be suitable for imaging AA in zebrafish.

3.6 Toxicity of CDs-DB@Fe in mice

In view of the excellent biocompatibility of CDs-DB@Fe in zebrafish, BALB/c mice were selected as the models for evaluating the toxicity of CDs-DB@Fe *in vivo*. First, a $200 \mu\text{L}$ PBS solution ($\text{pH} = 7.4$) was injected into the mice once a day by intravenous injections and this was continued for 30 days (control group). In addition, $200 \mu\text{L}$ CDs-DB@Fe (0.4 mg kg^{-1}) was injected into a separate group of mice once a day by intravenous injections and this was continued for 30 days (experimental group). Then, the mice were sacrificed, and the main tissues and organs were removed for H&E staining. The CDs-

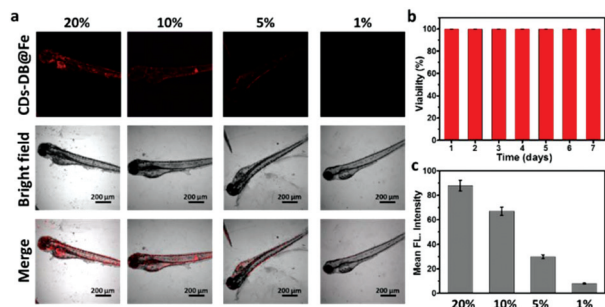


Fig. 4 Fluorescence images for monitoring AA under hypoxia stress in zebrafish via CDs-DB@Fe. (a) The zebrafish were pretreated with 20%, 10%, 5%, and 1% O_2 for 4 h, incubated with CDs-DB@Fe (0.1 mg mL^{-1}) for 1 h at 28°C , and washed with PBS ($\text{pH} 7.4$) to remove the remaining CDs-DB@Fe. (b) The toxicity of CDs-DB@Fe for zebrafish in 7 days. (c) The mean fluorescence intensity of part a. The emission was collected from 450 to 550 nm upon excitation at 405 nm.

DB@Fe-treated group and PBS group exhibited no distinct damage against the normal tissues (heart, liver, spleen, lung and kidney) (Fig. 5b). Hence, it was clear that CDs-DB@Fe had low toxicity and unobvious side effects *in vivo*.

3.7 Fluorescence imaging of liver ischemia tissue

In an actual biological sample, ischemia is the main reason for hypoxia. Therefore, AA in the ischemia organs should be evaluated to expand the application of our nanoprobe. The liver ischemia mice were selected as the test model. The liver was persistently ischemic for 5 min, 10 min, 30 min and 60 min by closing the portal vein with a non-invasive vascular clip. The mice without any treatment were used as the control group. All mice were sacrificed, and the normal liver tissue

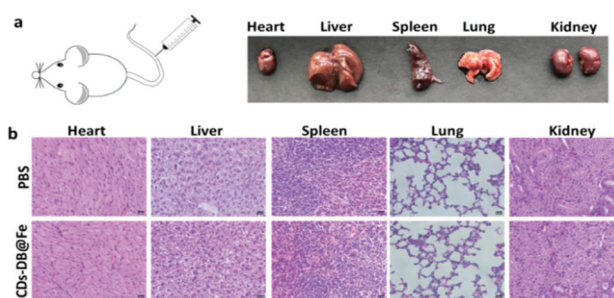


Fig. 5 Evaluation of the toxicity of CDs-DB@Fe in mice. (a) The schematic diagram and main organs (heart, liver, spleen, lung and kidney) of the mice model. (b) H&E staining of the normal tissues (heart, liver, spleen, lung and kidney). Magnification: $\times 400$. Data are presented as mean \pm SD ($n = 5$).

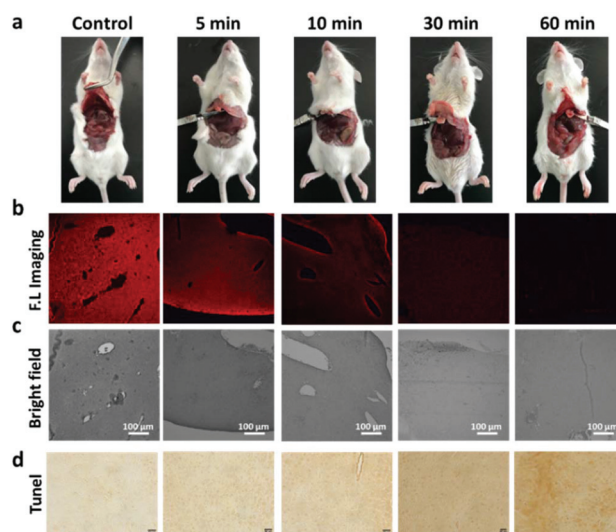


Fig. 6 Fluorescence imaging and TUNEL staining of liver ischemia tissues. (a) The details of the portal vein ligation with different times. (b) Fluorescence images of liver tissue section by a laser scanning confocal microscope. The emission was collected from 450 to 550 nm upon excitation at 405 nm. (c) The bright field of liver tissue section. (d) TUNEL staining of liver tissues in different groups. Data are presented as mean \pm SD ($n = 5$).

and ischemic liver tissue treated for different times were dissected for frozen sections. Next, the liver ischemia tissue sections were incubated with 0.1 mg mL⁻¹ CDs-DB@Fe for 1 h at 4 °C. Then, the stained sections were imaged by a laser scanning confocal microscope. As shown in Fig. 6b, the control group displays a strong fluorescence signal, and the ischemic liver tissue displays weak fluorescence. As the ischemia time increased, the fluorescence signal became weaker, indicating that CDs-DB@Fe could respond to AA in the liver ischemia mice model. TUNEL staining of the ischemic liver tissue was used to confirm the liver damage (Fig. 6d). These results suggested that AA decreased in the ischemia-induced hypoxic tissues and persistent ischemia could damage healthy tissues.

4. Conclusions

In summary, we successfully developed a fluorescent nanoprobe CD-DB by connecting CDs and desferrioxamine B for the associated detection of Fe³⁺ and AA. CD-DB exhibited outstanding sensitivity and selectivity towards Fe³⁺ and AA. The bioassays fully demonstrated that CD-DB could associatively detect additional Fe³⁺ and AA in living cells. Furthermore, CDs-DB@Fe could successfully determine the fluctuation of AA in hypoxic cell models and hypoxic zebrafish models. Moreover, a liver ischemia-induced hypoxic mice model was established to monitor the changes in AA. These results indicated that AA was consumed in various hypoxic models as AA could neutralize the hypoxia-induced free radicals and relieve oxidative stress. As far as we know, this is the first time that a CD-based nanoprobe has been applied to analyze the changes in AA in a hypoxic biological sample. In addition, our nanoprobe also exhibited low toxicity for living cells, zebrafish and mice. Overall, our nanoprobe as an ideal nanoagent has a great potential to understand the physiological effect of AA.

Conflicts of interest

There are no conflicts to declare.

Acknowledgements

We thank the National Nature Science Foundation of China (No. 21575159, 81573393, 21575080, 21976209), the program of Youth Innovation Promotion Association, CAS (Grant 2017256), the Instrument Developing Project of the Chinese Academy of Sciences (YZ201662).

References

- 1 S. R. Lynch, *Nutr. Rev.*, 1997, **4**, 102–110.
- 2 P. Aisen, M. Wessling-Resnick and E. A. Leibold, *Curr. Opin. Chem. Biol.*, 1999, **2**, 200–206.
- 3 R. S. Eisenstein, *Annu. Rev. Nutr.*, 2000, **20**, 627–662.
- 4 S. Al-Karadaghi, M. Hansson, S. Nikonov, B. Jonsson and L. Hederstedt, *Structure*, 1997, **11**, 1501–1510.
- 5 B. Halliwell, *J. Neurochem.*, 1992, **5**, 1609–1623.
- 6 S. Swaminathan, V. A. Fonseca, M. G. Alam and S. V. Shah, *Diabetes Care*, 2007, **7**, 1926–1933.
- 7 D. Galaris, V. Skiada and A. Barbouti, *Cancer Lett.*, 2008, **1**, 21–29.
- 8 O. K. Fix and K. V. Kowdley, *Minerva Med.*, 2008, **6**, 605–617.
- 9 V. Montecinos, P. Guzman, V. Barra, M. Villagran, C. Munoz-Montesino, K. Sotomayor, E. Escobar, A. Godoy, L. Mardones, P. Sotomayor, C. Guzman, O. Vasquez, V. Gallardo, B. van Zundert, M. R. Bono, S. A. Onate, M. Bustamante, J. G. Carcamo, C. I. Rivas and J. C. Vera, *J. Biol. Chem.*, 2007, **21**, 15506–15515.
- 10 A. C. Mamede, A. S. Pires, A. M. Abrantes, S. D. Tavares, A. C. Goncalves, J. E. Casalta-Lopes, A. B. Sarmiento-Ribeiro, J. M. Maia and M. F. Botelho, *Nutr. Cancer*, 2012, **7**, 1049–1057.
- 11 M. L. Heaney, J. R. Gardner, N. Karasavvas, D. W. Golde, D. A. Scheinberg, E. A. Smith and O. A. O'Connor, *Cancer Res.*, 2008, **19**, 8031–8038.
- 12 J. Verrax and P. B. Calderon, *Biochem. Pharmacol.*, 2008, **12**, 1644–1652.
- 13 A. S. Pires, C. R. Marques, J. C. Encarnacao, A. M. Abrantes, A. C. Mamede, M. Laranjo, A. C. Goncalves, A. B. Sarmiento-Ribeiro and M. F. Botelho, *Eur. J. Cell Biol.*, 2016, **6–7**, 208–218.
- 14 M. Fiorani, C. Azzolini, A. Guidarelli, L. Cerioni and O. Cantoni, *Pharmacol. Res.*, 2014, **84**, 12–17.
- 15 M. Pischetsrieder, *J. Agric. Food Chem.*, 1996, **8**, 2081–2085.
- 16 G. L. Simpson and B. J. Ortwerth, *Biochim. Biophys. Acta*, 2000, **1**, 12–24.
- 17 I. Nemet and V. M. Monnier, *J. Biol. Chem.*, 2011, **43**, 37128–37136.
- 18 H. S. Jung, X. Chen, J. S. Kim and J. Yoon, *Chem. Soc. Rev.*, 2013, **14**, 6019–6031.
- 19 T. Ueno and T. Nagano, *Nat. Methods*, 2011, **8**, 642–645.
- 20 X. Li, X. Gao, W. Shi and H. Ma, *Chem. Rev.*, 2014, **1**, 590–659.
- 21 H. Peng, P. Liu, D. Lin, Y. Deng, Y. Lei, W. Chen, Y. Chen, X. Lin, X. Xia and A. Liu, *Chem. Commun.*, 2016, **61**, 9534–9537.
- 22 Z. Pu, M. Wang, Z. Kou, I. S. Amiin and S. Mu, *Chem. Commun.*, 2016, **86**, 12753–12756.
- 23 C. Wang, H. Lin, Z. Xu, Y. Huang, M. G. Humphrey and C. Zhang, *ACS Appl. Mater. Interfaces*, 2016, **10**, 6621–6628.
- 24 X. Sun, Q. Zhang, K. Yin, S. Zhou and H. Li, *Chem. Commun.*, 2016, **81**, 12024–12027.
- 25 H. C. Chang and J. A. Ho, *Anal. Chem.*, 2015, **20**, 10362–10367.
- 26 J. C. G. Esteves Da Silva and H. M. R. Goncalves, *TrAC, Trends Anal. Chem.*, 2011, **8SI**, 1327–1336.
- 27 S. Qu, X. Wang, Q. Lu, X. Liu and L. Wang, *Angew. Chem., Int. Ed.*, 2012, **49**, 12215–12218.

- 28 Y. Wu, P. Wei, S. Pengpumpkiat, E. A. Schumacher and V. T. Remcho, *Anal. Chem.*, 2015, **16**, 8510–8516.
- 29 E. Ju, Z. Liu, Y. Du, Y. Tao, J. Ren and X. Qu, *ACS Nano*, 2014, **6**, 6014–6023.
- 30 L. M. Shen, Q. Chen, Z. Y. Sun, X. W. Chen and J. H. Wang, *Anal. Chem.*, 2014, **10**, 5002–5008.
- 31 C. Yuan, B. Liu, F. Liu, M. Y. Han and Z. Zhang, *Anal. Chem.*, 2014, **2**, 1123–1130.
- 32 X. Jia, J. Li and E. Wang, *Nanoscale*, 2012, **18**, 5572–5575.
- 33 M. J. Krysmann, A. Kellarakis, P. Dallas and E. P. Giannelis, *J. Am. Chem. Soc.*, 2012, **2**, 747–750.
- 34 B. Kong, A. Zhu, C. Ding, X. Zhao, B. Li and Y. Tian, *Adv. Mater.*, 2012, **43**, 5844–5848.
- 35 L. Zhou, Y. Lin, Z. Huang, J. Ren and X. Qu, *Chem. Commun.*, 2012, **8**, 1147–1149.
- 36 H. Li, J. Zhai and X. Sun, *Langmuir*, 2011, **8**, 4305–4308.
- 37 H. Li, J. Zhai, J. Tian, Y. Luo and X. Sun, *Biosens. Bioelectron.*, 2011, **12**, 4656–4660.
- 38 Q. Qu, A. Zhu, X. Shao, G. Shi and Y. Tian, *Chem. Commun.*, 2012, **44**, 5473–5475.
- 39 J. M. Liu, L. P. Lin, X. X. Wang, S. Q. Lin, W. L. Cai, L. H. Zhang and Z. Y. Zheng, *Analyst*, 2012, **11**, 2637–2642.
- 40 S. Liu, J. Tian, L. Wang, Y. Zhang, X. Qin, Y. Luo, A. M. Asiri, A. O. Al-Youbi and X. Sun, *Adv. Mater.*, 2012, **15**, 2037–2041.
- 41 H. X. Zhao, L. Q. Liu, Z. D. Liu, Y. Wang, X. J. Zhao and C. Z. Huang, *Chem. Commun.*, 2011, **9**, 2604–2606.
- 42 W. Bai, H. Zheng, Y. Long, X. Mao, M. Gao and L. Zhang, *Anal. Sci.*, 2011, **3**, 243–246.
- 43 H. Li, Y. Zhang, L. Wang, J. Tian and X. Sun, *Chem. Commun.*, 2011, **3**, 961–963.
- 44 W. Shi, Q. Wang, Y. Long, Z. Cheng, S. Chen, H. Zheng and Y. Huang, *Chem. Commun.*, 2011, **23**, 6695–6697.
- 45 V. Raveendran, A. R. S. Babu and N. K. Renuka, *RSC Adv.*, 2019, **9**, 12070–12077.
- 46 M. Shamsipur, K. Molaei, F. Molaabasi, M. Alipour, N. Alizadeh, S. Hosseinkhani and M. Hosseini, *Talanta*, 2018, **183**, 122–130.
- 47 L. Shi, Z. Hou, C. Zhang, G. Zhang, Y. Zhang, C. Dong and S. Shuang, *Anal. Methods*, 2019, **11**, 669–676.
- 48 H. Xu, S. Zhou, J. Liu and Y. Wei, *RSC Adv.*, 2018, **8**, 5500–5508.
- 49 J. S. Anjali Devi, S. Salini, A. H. Anulekshmi, G. L. Praveen and G. Sony, *Sens. Actuators, B*, 2017, **246**, 943–951.
- 50 X. Guo, G. Yue, J. Huang, C. Liu, Q. Zeng and L. Wang, *ACS Appl. Mater. Interfaces*, 2018, **10**, 26118–26127.
- 51 M. Zheng, Z. Xie, D. Qu, D. Li, P. Du, X. Jing and Z. Sun, *ACS Appl. Mater. Interfaces*, 2013, **24**, 13242–13247.
- 52 D. Peng, L. Zhang, F. Li, W. Cui, R. Liang and J. Qiu, *ACS Appl. Mater. Interfaces*, 2018, **10**, 7315–7323.
- 53 X. Guo, J. Huang, Q. Zeng, Y. Wei, X. Liu and L. Wang, *J. Mater. Chem. B*, 2019, **7**, 2799–2807.
- 54 Z. Xie, X. Sun, J. Jiao and X. Xin, *Colloids Surf., A*, 2017, **529**, 38–44.
- 55 X. Pan, X. Wang, L. Wang, K. Xu, F. Kong and B. Tang, *Anal. Chem.*, 2015, **14**, 7092–7097.
- 56 G. Horstick, T. Kempf, M. Lauterbach, M. Ossendorf, L. Kopacz, A. Heimann, H. A. Lehr, S. Bhakdi, J. Meyer and O. Kempfski, *J. Surg. Res.*, 2000, **1**, 28–34.